

MAPbBr₃ First-Order Distributed Feedback Laser with High Stability

Cheng Chang, Yangwei Shi, Chen Zou, and Lih Y. Lin*

A green-emitting perovskite first-order distributed feedback (DFB) laser based on the methylammonium lead bromide (MAPbBr₃) with high stability is demonstrated for the first time. The laser achieves stable lasing at 550 nm with a full width at half maximum of 0.4 nm. Low lasing threshold of 60 $\mu\text{J cm}^{-2}$ under nanosecond pulsed excitation and 3.1 $\mu\text{J cm}^{-2}$ under femtosecond pulsed excitation is observed, showing a much lower lasing threshold compared with the second-order DFB cavities, which are fabricated on the same substrate. By optimizing the antisolvent treatment and encapsulating with poly(methyl methacrylate), the laser lifetime, resistance to moisture, lasing threshold, and intensity are significantly improved. The lasers are fabricated with a complementary metal-oxide-semiconductor-compatible process, thus offer promising potential for the integrated photonic devices.

1. Introduction

Metal-halide perovskites are promising solution-processed materials with superior optical and electrical properties. Their high absorption coefficients, high-photoluminescence quantum yield (PLQY), low-trap-state densities, high carrier mobility, and tunable direct bandgaps are favorable for many optoelectronic devices such as light-emitting diodes (LEDs),^[1–3] solar cells,^[4–6] photodetectors,^[7,8] and optically pumped lasers.^[9,10] Recently, the efficiency for perovskite solar cells and LEDs has reached 25.8%^[11] and >28%,^[12,13] respectively. Room temperature continuous-wave lasing in quasi-2D perovskite second-order distributed feedback (DFB) laser has also been achieved,^[10] showing a promising future

for electrically pumped perovskite lasers. Conventional semiconductor lasers cover the spectrum from UV to near-IR well except the “green gap.” Given the facile emission color tunability of perovskite materials over the entire visible spectrum, perovskite lasers are promising for bridging this gap.

There are several types of perovskite lasers such as Fabry–Pérot resonators,^[14] photonic crystal lasers,^[15] random lasers,^[16] vertical-cavity surface-emitting lasers,^[17] and DFB lasers.^[18–20] Among them, first-order DFB lasers are especially favorable for integrated photonics with controllable lasing wavelength, small device structure, horizontal lasing direction, and edge-emitting wave-

guide output coupling. However, first-order perovskite DFB lasers have not been reported until recently; a red-emitting DFB laser based on the MAPbI₃ fabricated by nanoimprint lithography achieved a lasing threshold of 310 $\mu\text{J cm}^{-2}$ and full width at half maximum (FWHM) of 1.2 nm.^[21]

In this article, we demonstrated a green-emitting perovskite first-order DFB laser with low lasing threshold, narrow FWHM, high resistance to moisture, and long-term stability. The laser was fabricated on a silicon wafer with a complementary metal-oxide-semiconductor-compatible process. **Figure 1** shows the scanning electron microscope (SEM) images (Figure 1a,b) and a schematic illustration (Figure 1d) of the device. To facilitate detection of the laser output, second-order DFB gratings are utilized at both ends of the first-order DFB grating to couple the laser light out vertically. Those edge second-order DFB gratings were not capable of generating lasing but only facilitated light extraction, as shown in Figure S2, Supporting Information. Figure 1c shows the dark field image of the first-order DFB laser under operation. Upon nanosecond pulsed laser excitation which illuminates the first-order DFB grating area only, the laser achieved a narrow FWHM of 0.4 nm and a threshold of 60 $\mu\text{J cm}^{-2}$. This threshold value is about 60% lower than the second-order DFBs with the same design. The laser also shows long-term stability and moisture resistance with the encapsulation of a Poly(methyl methacrylate) (PMMA) layer. During a 4 h pumping process, the emission spectrum shows no change in FWHM and minor degradation in peak intensity.

C. Chang, L. Y. Lin
Department of Electrical and Computer Engineering
University of Washington
Seattle, WA 98195, USA
E-mail: lylin@uw.edu

Y. Shi
Molecular Engineering & Science Institute
University of Washington
Seattle, WA 98195, USA

C. Zou
State Key Laboratory of Modern Optical Instrumentation
College of Optical Science and Engineering
Zhejiang University
Hangzhou, Zhejiang 310027, China

 The ORCID identification number(s) for the author(s) of this article can be found under <https://doi.org/10.1002/adpr.202200071>.

© 2022 The Authors. Advanced Photonics Research published by Wiley-VCH GmbH. This is an open access article under the terms of the Creative Commons Attribution License, which permits use, distribution and reproduction in any medium, provided the original work is properly cited.

DOI: 10.1002/adpr.202200071

2. Results and Discussion

2.1. ASE and Lasing Performance

The details of device design and fabrication are shown in the supporting information. The experimental setup for measuring

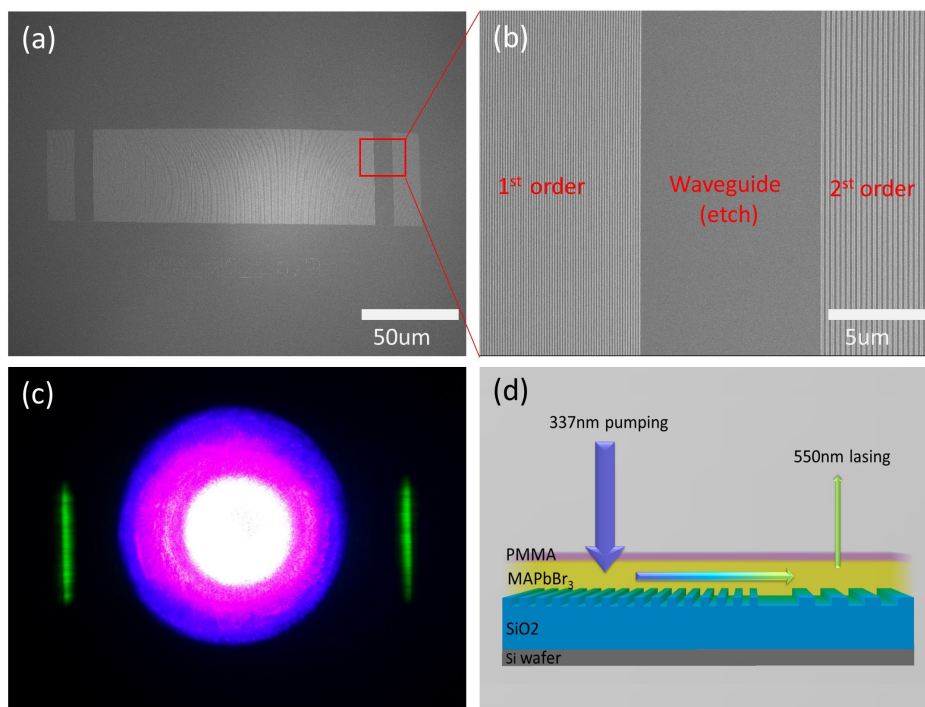


Figure 1. a) SEM image of the first-order DFB grating for the perovskite laser with b) a second-order DFB grating area for output coupling. A waveguide region without gratings separates the output-coupling grating from the first-order DFB resonator. c) Dark-field optical microscope image of the first-order perovskite DFB laser under operation. The image shows the pumping light illuminating the first-order DFB grating region, and the green emission coupled out of the second-order DFB gratings at both ends. d) Schematic illustration of the perovskite first-order DFB laser.

the amplified spontaneous emission (ASE) and lasing is described in Experimental Section. A nanosecond pulsed laser with 337 nm wavelength, 20 Hz repetition rate, and 3.5 ns pulse width was used as the pumping source, unless otherwise specified. All measurements were done at room temperature with an ambient environment.

The ASE was obtained by pumping the area without DFB gratings. **Figure 2a,b** shows the evolution of the ASE spectrum versus pump fluence. At low excitation, the photoluminescence (PL) spectrum shows an FWHM of 21 nm around a 530 nm emission peak. After the pump fluence is increased to around $400 \mu\text{J cm}^{-2}$, the FWHM is reduced to 2 nm and the emission peak shifts to 550 nm, both indicating the onset of ASE. The red shift is attributed to the transition from a higher-energy bound exciton state (PL) to a lower-energy bound exciton state (ASE).^[22] Under high pump fluence, the higher-energy state serves as the optical pump for the lower-energy state; thus, the ASE emission at 550 nm dominates.

We then moved the pump light to the first-order DFB grating region and performed the measurements again. The results shown in **Figure 2c,d** clearly indicate lasing of the perovskite laser. The emission spectrum shows a steep drop in FWHM once the pump fluence reaches a lasing threshold of $\approx 60 \mu\text{J cm}^{-2}$. We also fabricated the first-order DFB gratings with different periods ranging from 138 to 144 nm. The emission spectra of the perovskite lasers with these DFB gratings are shown in **Figure 2e**. The lasing wavelength is tuned from 546.9 to 556.8 nm, corresponding to the grating period change which affects the effective refractive index as well.

Compared to the lasing threshold reported in other prior works using picosecond and femtosecond pulsed pumping,^[10,19,20] the lasing threshold shown in this work is higher as a nanosecond pulsed laser was used as the pumping source. Stimulated emission lifetime is shorter than Auger recombination lifetime, typically in the range of picoseconds. Our pumping source's 3.5 ns laser pulse is much longer than the stimulated emission lifetime, thus leading to a significant heat accumulation issue. To provide a comparable baseline, lasing performance was also tested with a femtosecond laser (400 nm wavelength, 50 kHz repetition rate, and 100 fs pulse width), showing a low threshold of $\approx 3.4 \mu\text{J cm}^{-2}$ in **Figure S3**, Supporting Information.

To compare the lasing threshold of the first-order DFB lasers with the second-order DFB lasers, we fabricated both first- and second-order DFB gratings on the same substrate with the same processing conditions. Lasing thresholds of $69.5 \mu\text{J cm}^{-2}$ for the first-order DFB laser and $168.6 \mu\text{J cm}^{-2}$ for the second-order DFB laser were observed (**Figure 2f**), which are in accordance with the theory that the lasing threshold for the first-order DFB lasers should be reduced by a factor of 2 compared with the second-order DFB lasers.^[23]

2.2. Antisolvent Treatment

The antisolvent method has been widely used for preparing the high-quality low-defect perovskite films in the application of solar cells, photodetectors, and LEDs.^[24] Common antisolvents for MAPbBr₃ are chlorobenzene (CB) and toluene (Tol) due to their insolubility of perovskites and miscibility with the precursor

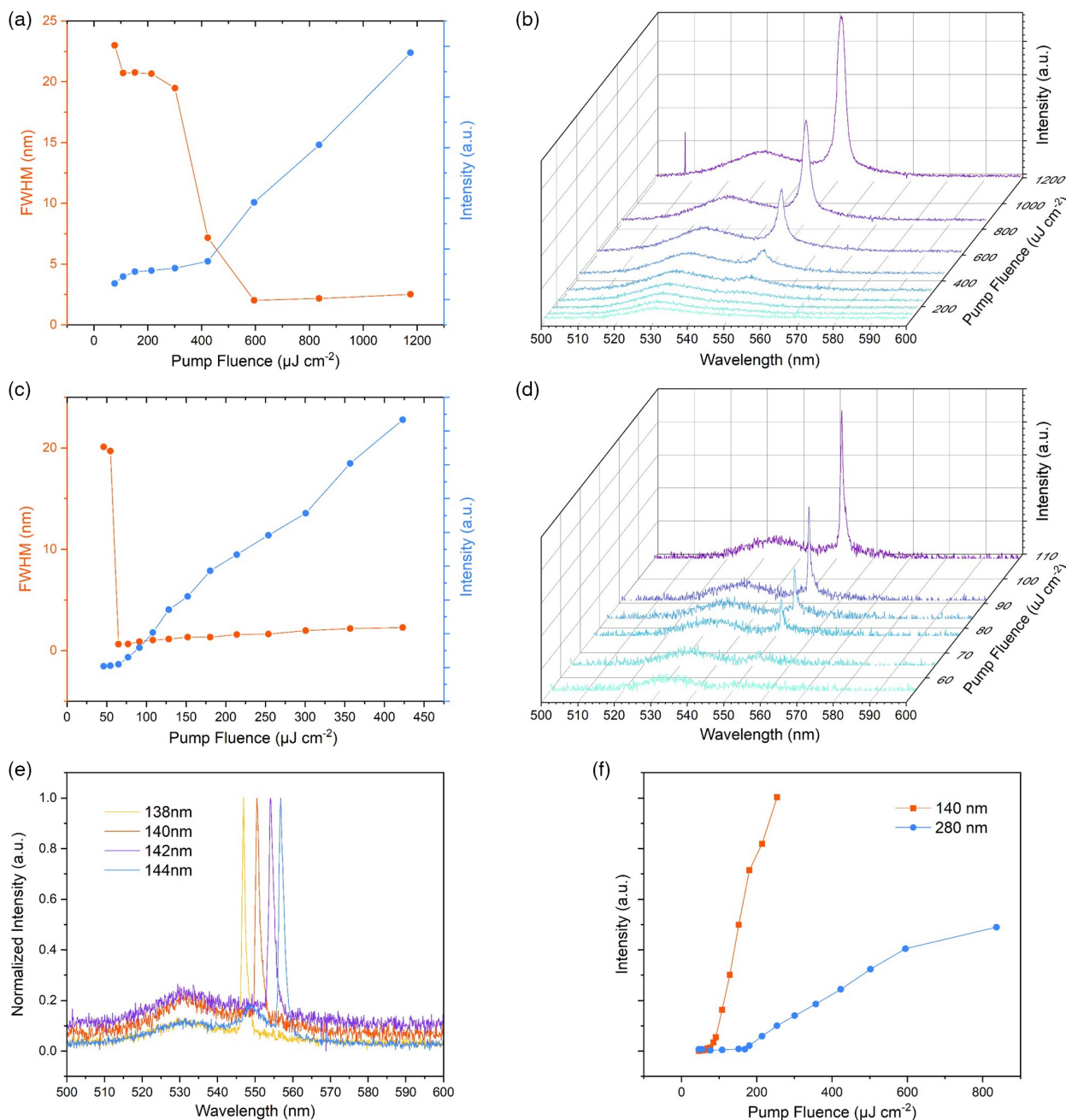


Figure 2. a) FWHM and ASE intensity as a function of pump fluence. b) Evolution of the ASE emission spectrum versus increasing pump fluence. c) FWHM and laser output intensity as a function of pump fluence. d) Evolution of emission spectra under different pump fluences. e) Dependence of the lasing peak wavelength on the grating period of the first-order DFB lasers. f) Comparison between the laser output intensity of the first- and second-order DFB lasers.

solvent (dimethyl sulfoxide (DMSO)/N,N-dimethylformamide (DMF)). The antisolvents are added during spin coating right before perovskite crystallization. During the process, antisolvents mix with the perovskite precursor, extract the precursor solvent, and form local supersaturation for perovskites, forcing the material to quickly recrystallize.^[25] It is reported that the antisolvent with high boiling points and good miscibility with DMSO/DMF is favorable. A list of several commonly used antisolvents and their properties is shown in Table S2, Supporting

Information. We tested multiple antisolvents (ethyl acetate (EA), methyl acetate (MA), Tol, CB, and hexane) and demonstrated that, by applying the EA as antisolvent, the laser performance can be best improved. All the results shown previously were based on EA antisolvent treatment.

Figure 3a shows the light-in versus light-out characterization results (L–L curve) for the first-order perovskite DFB lasers fabricated using different antisolvents. The lasing thresholds for EA, MA, Tol, and CB-treated devices are around 60, 95, 110, and

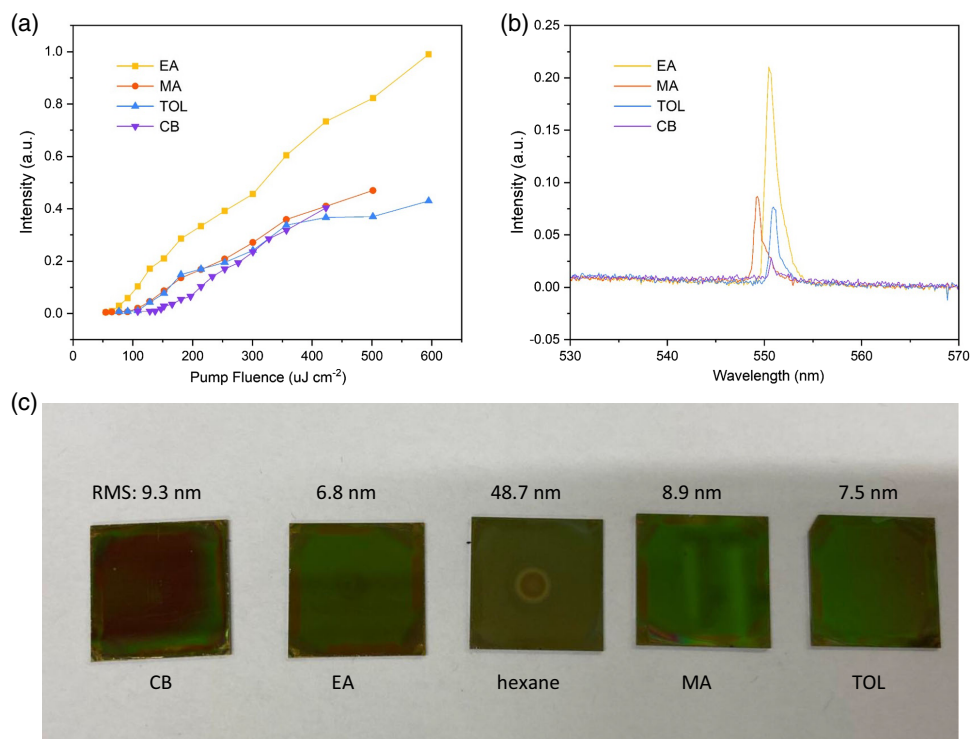


Figure 3. a) First-order perovskite DFB lasers fabricated using different antisolvents. (a) L–L curve and b) laser emission spectrum under $152 \mu\text{J cm}^{-2}$ nanosecond pulsed pumping. c) Images of laser samples using different antisolvents with their surface roughness.

$147 \mu\text{J cm}^{-2}$, respectively. In the high pump fluence region, the laser intensity for MA, Tol, and CB-treated devices is similar due to saturation, whereas the EA-treated device shows twice the intensity of the others. Figure 3b presents the lasing spectra of devices with MAPbBr_3 films using different antisolvents under nanosecond pulsed pumping with a pump fluence of $152 \mu\text{J cm}^{-2}$, the peak intensity and wavelength clearly vary. Figure 3c shows the film morphology and surface roughness of each device. All devices have a smooth and glossy surface except the hexane-treated sample, where no lasing or ASE was detected due to high-film roughness. We think the photon scattering and recombination would cause different lasing threshold levels. The various antisolvents have different boiling points and polarity, so the crystallization rate would be significantly discrepant, which could lead to different surface morphology. Rough films may have large scattering loss, which increases the lasing threshold. The PL spectrum and time-resolved photoluminescence measurement of each antisolvent treated film are shown in Figure S7 and S8, Supporting Information.

2.3. Laser Stability

Solving the stability issue of solution-processed perovskite lasers is still a key challenge. It is well known that perovskite materials degrade due to the chemical reaction with oxygen and moisture easily. Especially under the condition of high-power pumping, the accumulated joule heating accelerates the decomposition process, thus decreasing the laser performance. Ligand modification for perovskite quantum dots (QDs),^[26,27] hydrophobic

organic-layer engineering,^[28] and perovskite QD-embedded polyacrylonitrile^[29] have all been proved to be effective methods to prolong the laser's lifetime by isolating the perovskite gain materials from the air.

Here, we show that with a thin layer of PMMA on top of the perovskite layer, the device performance and lifetime can be significantly improved. After the perovskites were spin-coated and annealed, PMMA in Tol solution was spin-coated on the device and annealed. As Tol is an antisolvent for perovskites, it does not react with the perovskite layer. However, as PMMA has a refractive index between MAPbBr_3 and air ($n_{\text{PMMA}} = 1.5$, $n_{\text{MAPbBr}_3} = 2.2$, $n_{\text{air}} = 1$), it acts as an index ladder and reduces light confinement, as shown in Figure S4, Supporting Information. The potential effect of this on the quality factor can be mitigated by revising the DFB grating structure to increase the overlap between the laser mode profile and the grating.

To compare the performance of the devices with and without PMMA encapsulation, we excite the lasers at a pump fluence of $2P_{\text{th}}$, where P_{th} is the lasing threshold, using the nanosecond pulsed laser. As shown in Figure 4a, the unencapsulated device's output intensity quickly dropped to 60% of the initial value after about 10 min. The device encapsulated with PMMA showed stable lasing for 4 h (288 000 laser shots) with almost no FWHM broadening (Figure 4a,b). The laser output spectra in Figure 4b also show that the laser peak intensity maintained $\approx 82\%$ of its initial value after 4 h with a minor blue shift of $\approx 0.3 \text{ nm}$. In contrast, the unencapsulated device only maintained 35% of the initial intensity and emission peak blue shifted 1.7 nm (Figure 4c). It is interesting to note that there is a slight intensity increase in the first several minutes of pumping for the

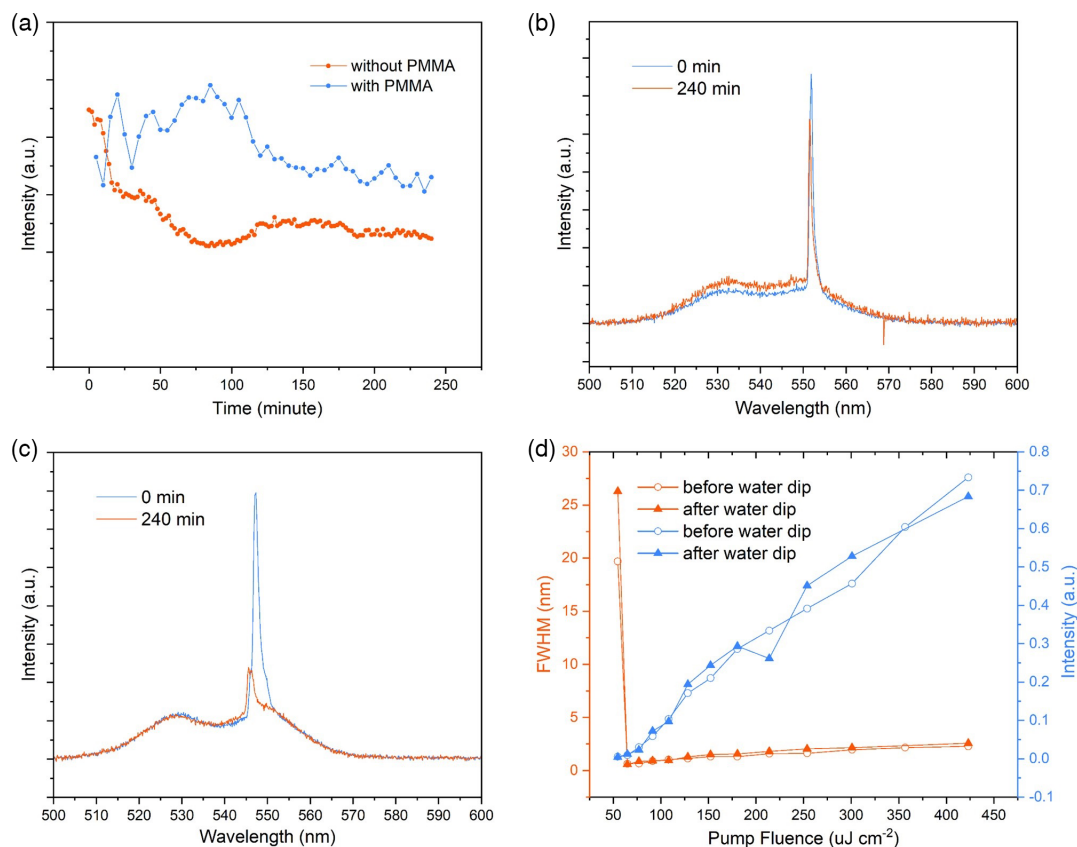


Figure 4. a) Laser intensity over time under optical pumping at twice the lasing threshold. The lasing spectrum of b) the PMMA-encapsulated device and c) the unencapsulated device at the beginning and end of the 4 h measurement. d) Laser performance before and after dipping into water.

encapsulated device, but the PL intensity remains the same during the process (Figure S9, Supporting Information). The increase was not very obvious for the unencapsulated device due to quick degradation. The phenomenon is also observed in similar works.^[17,30,31] This may be due to some self-healing effects of perovskites under optical pumping that smoothen the surface.

A sample was stored in air for a week and measured again. The results before and after storage are shown in Figure S5, Supporting Information, showing no degradation in the laser performance.

To accelerate the degradation effect from moisture, we dipped the device in water briefly and then compared its performance in FWHM and L–L characteristics (Figure 4d). The performance was almost identical before and after the dip, showing that the PMMA layer provided sufficient protection against moisture. The perovskite layer in devices without PMMA encapsulation dissolved immediately in water; therefore, further testing was not possible for these devices.

3. Conclusions

In summary, we designed, fabricated, and optimized first-order DFB lasers based on MAPbBr₃, which shows around 60% decrease in lasing threshold compared with the second-order DFB lasers. Utilizing EA as the antisolvent, the lasing threshold

was reduced significantly to 60 $\mu\text{J cm}^{-2}$ under nanosecond pulse pumping, and the optical output intensity was substantially higher than that of lasers treated with other antisolvents. Laser emission FWHM as narrow as 0.4 nm was achieved. The peak wavelength can be tuned from 546.9 to 556.8 nm by changing the first-order DFB grating period. With a thin PMMA layer encapsulation, the laser performance and stability can be greatly improved. The results demonstrate the promising prospect of perovskite DFB lasers in filling the green gap of semiconductor lasing sources for integrated photonics.

4. Experimental Section

Materials: MABr (>99.5% purity) was purchased from Ossila. PbBr₂ (99.9%, metal basis), PMMA ($\approx 120\,000$ MW), and DMSO (anhydrous) were purchased from Sigma Aldrich. DisCharge (2 \times) was purchased from DisChem.

DFB Gratings Fabrication: Silicon substrates with 2 μm wet thermal oxide were cleaned by ultrasonication using detergent, acetone, isopropanol, and DI water, followed by plasma cleaning at 150 W for 3 min. A 110 nm layer of ZEP520A Ebeam lithography resist was spin-coated on the substrates and annealed at 180 $^{\circ}\text{C}$ for 3 min. Then, a DisCharge layer was spin-coated on the resist at 4000 rpm. Electron beam lithography was performed to draw grating patterns on the resist layer using a JBX-6300FS system (JEOL) with an optimized dose of 185 $\mu\text{C cm}^{-2}$. After the exposure, the substrates were submerged in water for 1 min to strip the DisCharge. Amyl acetate was used to develop the patterns at room temperature. The patterned resist layer was used as the etching mask in an inductively coupled

plasma fluorine etcher to etch 60 nm of silicon dioxide. Finally, the substrates were heated in N-methyl-2-pyrrolidone at 90 °C overnight to strip the resist.

Solutions Synthesis: The green perovskite precursor was obtained by mixing 0.84 M MABr and 0.8 M PbBr₂ (MABr : PbBr = 1.05 : 1) in DMSO. The precursor was heated at 60 °C for 12 h with constant stirring. After cooling to room temperature, the precursor was filtered with 0.45 μm PTFE filters. The encapsulation layer was prepared by dissolving 20 mg of PMMA in 1 mL of Tol and stirring for sufficient time.

Device Fabrication: The silicon substrates with DFB gratings were cleaned as previously described. Then, the substrates were treated by ultraviolet plasma cleaning to increase wettability. Precursor solution of MAPbBr₃ was spin-coated on the substrate at 3000 rpm for 1 min in a nitrogen-filled glove box. 200 μL of antisolvent was dropped onto the substrate during spin coating to accelerate nucleation. Then, the substrates were baked at 60 °C for 10 min. PMMA in Tol was spin-coated on the perovskite layer as an encapsulation layer, and then annealed for another 10 min.

ASE and Lasing Measurement: For both ASE and lasing measurement, the samples were pumped by a nanosecond nitrogen laser (337 nm, 20 Hz, 3.5 ns pulse width; NL 100, Stanford Research System) with a micro-PL system. The pump fluence was tuned by a continuously variable neutral-density filter. Both the excitation light and PL were vertically coupled in/off the sample. A cascaded 4-f imaging system in conjunction with a 450 nm long-pass filter was used to collect the emission before a spectrometer (Thorlabs CCS100) and a charge-coupled device camera.

Supporting Information

Supporting Information is available from the Wiley Online Library or from the author.

Acknowledgements

This work was supported by the National Science Foundation (grant ECCS-1807397) and the University of Washington Royalty Research Fund. Part of device fabrication was conducted at the Washington Nanofabrication Facility, a National Nanotechnology Coordinated Infrastructure site at the University of Washington supported by the National Science Foundation (grant NNCI-1542101). We acknowledge Prof. David S. Ginger for his support, encouragement, and use of facilities to pursue this work. Yangwei Shi thanks the financial support from the Office of Naval Research (ONR), Award Number N00014-20-1-2587.

Conflict of Interest

The authors declare no conflict of interest.

Data Availability Statement

The data that support the findings of this study are available from the corresponding author upon reasonable request.

Keywords

antisolvents, first-order DFB lasers, MAPbBr₃, perovskites, stability

Received: April 14, 2022

Revised: August 1, 2022

Published online:

- [1] K. Lin, J. Xing, L. N. Quan, F. P. Arquer, X. Gong, J. Lu, L. Xie, W. Zhao, D. Zhang, C. Yan, W. Li, X. Liu, Y. Lu, J. Kirman, E. H. Sargent, Q. Xiong, Z. Wei, *Nature* **2018**, 562, 245.
- [2] K. Zhang, N. Zhu, M. Zhang, L. Wang, J. Xing, *J. Mater. Chem. C* **2021**, 9, 3795.
- [3] C. Zou, Y. Liu, D. Ginger, L. Lin, *ACS Nano* **2020**, 14, 6076.
- [4] W. Yin, T. Shi, Y. Yan, *Appl. Phys. Lett.* **2014**, 104, 063903.
- [5] E. Sanehira, A. Marshall, J. Christians, S. Harvey, P. Ciesielski, L. Wheeler, P. Schulz, L. Lin, M. Beard, J. Luther, *Sci. Adv.* **2017**, 3, eaao4204.
- [6] S. Stranks, H. Snaith, *Nat. Nanotechnol.* **2015**, 10, 391.
- [7] L. Dou, Y. Yang, J. You, Z. Hong, W. Chang, G. Li, Y. Yang, *Nat. Commun.* **2014**, 5, 5404.
- [8] C. Zou, Y. Xi, C. Huang, E. Keeler, T. Feng, S. Zhu, L. Pozzo, L. Lin, *Adv. Opt. Mater.* **2018**, 6, 1800324.
- [9] C. Zou, C. Zhang, Y. Kim, L. Lin, J. Luther, *ACS Photonics* **2021**, 8, 386.
- [10] C. Qin, A. Sandanayaka, C. Zhao, T. Matsushima, D. Zhang, T. Fujihara, C. Adachi, *Nature* **2020**, 585, 53.
- [11] H. Min, D. Lee, J. Kim, G. Kim, K. Lee, J. Kim, M. Paik, Y. Kim, K. Kim, M. Kim, T. Shin, S. Il Seok, *Nature* **2021**, 598, 444.
- [12] Y. Shen, L. Cheng, Y. Li, W. Li, J. Chen, S. Lee, J. Tang, *Adv. Mater.* **2019**, 31, 1901517.
- [13] Z. Liu, W. Qiu, X. Peng, G. Sun, X. Liu, D. Liu, Z. Li, F. He, C. Shen, Q. Gu, F. Ma, H. Yip, L. Hou, Z. Qi, S. Su, *Adv. Mater.* **2021**, 33, 2103268.
- [14] H. Zhu, Y. Fu, F. Meng, X. Wu, Z. Gong, Q. Ding, M. Gustafsson, M. Trinh, S. Jin, X. Zhu, *Nat. Mater.* **2015**, 14, 636.
- [15] N. Pourdavoud, S. Wang, A. Mayer, T. Hu, Y. Chen, A. Marianovich, W. Kowalsky, R. Heiderhoff, H. Scheer, T. Riedl, *Adv. Mater.* **2017**, 29, 1605003.
- [16] Y. Wang, H. Li, Y. Hong, K. Hong, F. Cheng, C. Hsu, R. Lee, C. Conti, T. Kao, T. Lu, *ACS Nano* **2019**, 13, 5421.
- [17] C. Huang, C. Zou, C. Mao, K. Corp, Y. Yao, Y. Lee, C. Schlenker, A. Jen, L. Lin, *ACS Photonics* **2017**, 4, 2281.
- [18] Y. Jia, R. Kerner, A. Grede, B. Rand, N. Giebink, *Nat. Photonics* **2017**, 11, 784.
- [19] N. Pourdavoud, A. Mayer, M. Buchmüller, K. Brinkmann, T. Häger, T. Hu, R. Heiderhoff, I. Shutsko, P. Görrn, Y. Chen, H. Scheer, T. Riedl, *Adv. Mater. Technol.* **2018**, 3, 1700253.
- [20] J. Harwell, G. Whitworth, G. Turnbull, I. Samuel, *Sci. Rep.* **2017**, 7, 1.
- [21] S. Basak, O. Bar-On, J. Scheuer, *Opt. Mater. Express* **2022**, 12, 375.
- [22] D. Priante, I. Dursun, M. Alias, D. Shi, V. Melnikov, T. Ng, O. Mohammed, O. Bakr, B. Ooi, *Appl. Phys. Lett.* **2015**, 106, 081902.
- [23] C. Karnutsch, C. Gyrtner, V. Haug, U. Lemmer, T. Farrell, B. Nehls, U. Scherf, J. Wang, T. Weimann, G. Heliotis, C. Pflumm, J. deMello, D. Bradley, *Appl. Phys. Lett.* **2006**, 89, 201108.
- [24] L. Xu, S. Che, J. Huang, D. Xie, Y. Yao, P. Wang, P. Lin, H. Piao, H. Hu, C. Cui, F. Wu, D. Yang, X. Yu, *Appl. Phys. Lett.* **2019**, 115, 033101.
- [25] J. Sun, F. Li, J. Yuan, W. Ma, *Small Methods* **2021**, 5, 2100046.
- [26] D. Yan, T. Shi, Z. Zang, T. Zhou, Z. Liu, Z. Zhang, J. Du, Y. Leng, X. Tang, *Small* **2019**, 15, 1901173.
- [27] X. Tang, J. Yang, S. Li, Z. Liu, Z. Hu, J. Hao, J. Du, Y. Leng, H. Qin, X. Lin, Y. Lin, Y. Tian, M. Zhou, Q. Xiong, *Adv. Sci.* **2019**, 6, 1970107.
- [28] M. Li, Q. Gao, P. Liu, Q. Liao, H. Zhang, J. Yao, W. Hu, Y. Wu, H. Fu, *Adv. Funct. Mater.* **2018**, 28, 1707006.
- [29] L. Wang, L. Meng, L. Chen, S. Huang, X. Wu, G. Dai, L. Deng, J. Han, B. Zou, C. Zhang, H. Zhong, *J. Phys. Chem. Lett.* **2019**, 10, 3248.
- [30] S. Chen, C. Zhang, J. Lee, J. Han, A. Nurmikko, *Adv. Mater.* **2017**, 29, 1604781.
- [31] Y. Wang, X. Li, J. Song, L. Xiao, H. Zeng, H. Sun, *Adv. Mater.* **2015**, 27, 7101.